ISSN (Print) 1226-1750
ISSN (Online) 2233-6656
Journal of Magnetics 23(4), 570-577 (2018) https://doi.org/10.4283/JMAG.2018.23.4.570

Analysis of Direction and area of Magnetic Susceptibility Artifact according to Frequency-encoding Changes in 3.0 Tesla MRI

Ji-Won Kim[1], Wan-Sik Park[1], Hyun-Sung Kim[1], Soo-Chul Kim[1], Yoon-Heui Kang[2], Tae-Kun Kim[2], Dong-Kyoon Han[1], and Yeong-Cheol Heo[1]*

[1]*Department of Radiological Science, college of Health Science Eulji University, Seongnam 13135, Republic of Korea*
[2]*Department of Radiology, Bundang Cha Hospital, Seongnam 13479, Republic of Korea*

(Received 24 August 2018, Received in final form 24 October 2018, Accepted 24 October 2018)

In this study, the length and area of t he artifact were quantitatively evaluated according to the direction of the magnetic susceptibility artifact. Using a self-made magnetic susceptibility artifact phantom the frequency-encoding direction in the 3.0T MRI system was changed in axial, coronal, and sagittal planes using T2 fast spin echo (FSE). The results showed a difference in length when the frequency encoding was changed from antero-posterior (AP) to right-to-left (RL) in the axial, RL to superior-inferior (SI) in coronal and AP to SI in sagittal planes ($p < 0.05$). In addition, the difference occurred when the magnetic susceptibility artifact area was measured according to the frequency-encoding direction conversion ($p < 0.05$). However, additional studies of magnetic susceptibility artifacts using various types of screws and plates are needed. This study provides basic data to prevent magnetic susceptibility artifact due to screw fixation.

Keywords : frequency encoding, magnetic susceptibility artifact, distortion, screw fixation, MRI

1. Introduction

Surgical operations such as screw fixation have been performed for patients with fracture to minimize ligament and vascular injury [1, 2]. Magnetic resonance imaging (MRI) has been used to evaluate the risk of bone tissue destruction after screw fixation surgery [3, 4]. MRI is an imaging modality that converts electrical signals, generated by the magnetic field in the human body, into images [5, 6]. The 3.0T MRI is commonly used in clinical practice as it provides a high degree of contrast and resolution to enhance the diagnostic value of the image [7-10]. However, MRI also has a disadvantage due to image artifacts generated by hardware, software, magnetic field environment, and parameters [11, 12]. Diagnostic artifacts include misdiagnosis due to signal loss unlike the actual human anatomy [13]. Among them, magnetic susceptibility artifacts induce image distortion associated with altered magnetic susceptibility, for example, due to metals in the body causing nonuniform local magnetic field [14]. Especially, in the case of a patient with metallic implants and screws in the human body, signal loss occurs due to magnetic susceptibility artifact, which lowers the diagnostic value of the diagnostic image [15]. When artifact occurs in MRI, the direction of artifact varies depending on the direction of frequency and phase encoding since artifacts often occur in the direction of matrix alignment [16]. Many studies reported distortion of magnetic susceptibility artifacts, with inadequate investigation into quantitative directionality [17, 18].

Predetermination of quantitative directionality of susceptibility artifact before MRI may prevent the loss of diagnostic value due to artifact and facilitate the identification of regions of interest in the image.

Therefore, this study provides the basic data on directionality of magnetic susceptibility artifact, by quantifying the length and area of artifact.

2. Subjects and Methods

2.1. Phantom design

A self-generated phantom was designed for use in this study to identify magnetic susceptibility artifacts. Pig hind limb bones were surgically inserted in the 15 × 15 × 15 cm acrylic phantom using metal screws. The pig hind limb bones were placed in the center of the phantom

©The Korean Magnetics Society. All rights reserved.
*Corresponding author: Tel: +82-31-740-7351
Fax: +82-31-740-7134, e-mail: eehrrn@hanmail.net

© 2018 Journal of Magnetics

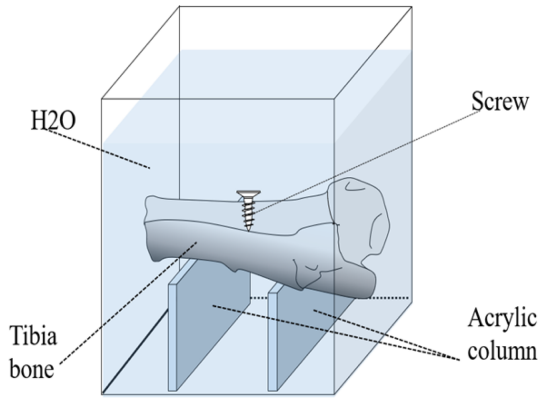

Fig. 1. (Color online) The phantom produced in this study was first inserted by a screw into the tibia of pig, and the tibia was screwed into the center of 15 × 15 × 15 cm acrylic box and filled with water. Finally, the phantom was scanned with the pig's tibia attached in the center in an acrylic box filled with water.

using a support. The phantom was filled with water and tissue equivalent material to mimic the human environment (Fig. 1).

2.2. Experimental method

In this study, we used SignaHDxT 3.0 T MRI system (GE healthcare), which is a whole- body MRI, and set the head region with 16 Channel Head Neck Spine Coil (HNS) (Fig. 2).

For image acquisition, T2 Fast Spin Echo (FSE) was used and the time image parameters used were as follows: Matrix size, 384 × 224; FOV, 160 mm; Gap, 0.3 mm; TE, 120; TR, 4000 msec; NEX, 2; and slice thickness, 3 mm.

Image acquisition in MRI is based on the principle of magnetization of hydrogen nuclei by placing a human body in a magnetic field, collection of signal information using a gradient coil, and image acquisition by Fourier transforming the collected signal. In this regard, S. Balac *et al.* [19] developed a mathematical model and numerical simulation of magnetic susceptibility artifact in MRI based on the Lamor relationship, to derive the resonant frequency required for signal acquisition. The Lamor relationship is as defined by the following equation.

$$V_L = \frac{\gamma}{2\pi} B \tag{1}$$

V_L means denotes the precessional frequency, $\frac{\gamma}{2\pi}$ is the gyromagnetic ratio, and B is the strength of the magnetic field. It can be seen that the precessional frequency changes with the intensity of the magnetic field.

MRI exhibits slice, frequency, and phase gradient. Among them, the section selected by slice gradient is as follows.

$$V_s = \frac{\gamma}{2\pi}|B_0 + G_s| = \frac{\gamma}{2\pi}(B_0 + g_s c) \tag{2}$$

V_s is the resonance frequency of the slice gradient, B_0 is the main magnetic field, and G_s is the slice selection gradient. Multiple sections of the resonant frequency can be selected by using resonance frequency and slice selection gradient.

Among the two gradients that collect signal information, the frequency-encoding gradient is expressed as follows.

$$V = \frac{\gamma}{2\pi}|B_0 + G_r| = \frac{\gamma}{2\pi}(B_0 + g_r x_r) \tag{3}$$

V is the frequency signal based on the frequency-encoding gradient, G_r is a frequency encoding gradient. B_0 means represents the primary magnetic field. The frequency gradient is used to acquire alternate signals.

The equation for phase encoding gradient is as follows.

$$\varnothing = 2\pi V_L(P)T_0 = \gamma|B_0 + G_0|T_0 = \gamma(B_0 + g_0 x_0)T_0 \tag{4}$$

$\varnothing$ is the phase of the collected signal based on the phase encoding gradient, G_0 is the phase encoding gradient. T_0 means denotes the time of onset of the phase encoding gradient. The phase gradient enables signal

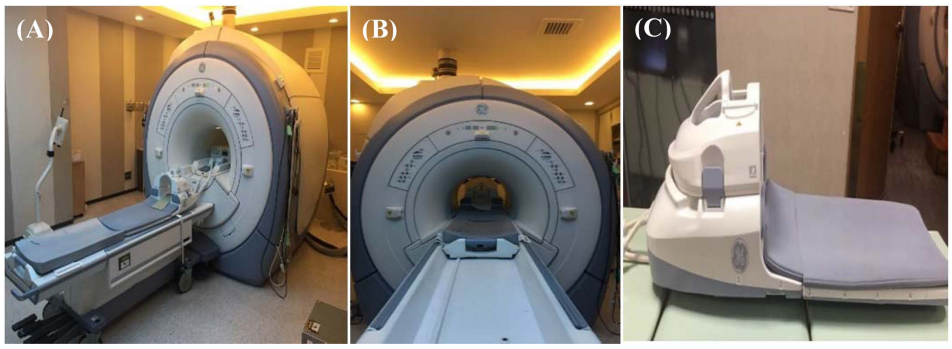

Fig. 2. (Color online) The equipment used in this study was as follows: GE Healthcare Signa HD xT3.0T (A), 16-channel HNS (head) coil (B) and experimental equipment with phantom (C).

collection by varying the intensity of the gradient.

The Fourier transform equation for collection and separation of the signals obtained is as follows.

$$G(f) = \int_{-\infty}^{\infty} g(t) e^{-f2\pi ft} \tag{5}$$

$G(f)$ means denotes the infinite sum of the sine wave and the simple cosine of the changing amplitude and the gradually increasing frequency f, and $g(t)$ stands for time for signal processing in various types of Fourier transform. The signals obtained through the Fourier transform are obtained as an image.

Patients with metallic implants in the body show magnetic susceptibility artifacts in the image. After MRI, non-uniformity of the magnetic field, band width, spin density, magnetic susceptibility, and gradient contribute to the generation of magnetic susceptibility artifact. Wenmiao Lu *et al.* [20] defined the factors contributing to the generation of magnetism-sensitive artifacts using the following equation.

$$m_e(\chi, z) = m(\chi, z) \cdot \prod \left[\frac{\frac{\gamma}{2\pi} G_s Z + \Delta f(\chi, z) - f_e}{B_{RF}} \right] \tag{6}$$

$m_e(\chi, z)$ represents the non-uniformity of the magnetic field induced in the metal, $m(\chi, z)$ is denotes spin density, $\frac{\gamma}{2\pi}$ is the gyromagnetic ratio of 1H, G_s is the amplitude of gradient, z is the direction of read out and desired slice selection, $\Delta f(\chi, z)$ represents non-uniform magnetic field, f_e is $\frac{\gamma}{2\pi} G_S Z_0$, and Z_0 indicates directions except for direction of the readout and slice selection. Magnetic susceptibility artifacts are altered by TE, material, phase shift, and so on. A. A. O. Carneiro *et al.* [21] defined the relationship with TE, which is a variable, using the following equation.

$$S_{SE} = S_0 \left[1 - 2e^{-\frac{TR - TE/2}{T_1}} + e^{-\frac{TE}{T_1}} \right] e^{-\frac{TE}{T_2}} \tag{7}$$

S_{SE} is represents spin echo indicating signal strength, S_0 is denotes proton density, T_1 stands for T_1 relaxation, T_2 is the T_2 relaxation, TE is the echo time, TR is repetition time, and e refers to natural logarithm. Since the signal strength changes according to TE, in order to minimize the effect of TE, TE was fixed to 60 msec in this study.

Venook *et al.* [22] defined the relationship between materials such as metallic implants and magnetic susceptible artifacts using the following equation.

$$\Delta\chi = \Delta\omega / \gamma G_r \propto \Delta X B_0 / G_r \tag{8}$$

$\Delta\chi$ indicates the size of the artifact depending on the material, $\Delta\omega$ represents frequency shift, γ is the gyromagnetic ratio, G_r is the size of readout gradient, and ΔX refers to susceptibility mismatch. Depending on the type of material, the size of the artifact is altered if susceptibility mismatch and readout gradient change. Therefore, the material is fixed with the titanium alloy in order to control the magnetic susceptibility artifact changes due to the material difference.

Karin Shmueli *et al.* [23] also defined the shift in magnetic susceptibility artifacts in the phase shift using the following equation.

$$\varnothing(X, Y, Z) = -\gamma \cdot B_0 \cdot TE \cdot FT^{-1}\left(\frac{1}{3} - \frac{K_Z^2}{K^2}\right) \otimes \chi(X, Y, Z) \tag{9}$$

$\chi(X, Y, Z)$ represents the magnetic susceptibility artifact, FT is Fourier transform, $\varnothing(X, Y, Z)$ is phase image, γ is proton gyromagnetic ratio, $B0$ is strength of the magnetic field, TE is echo time, K_Z is Z-axis vector of K-space parallel to the runner field, and K^2 is $K_x^2 + K_y^2 + K_z^2$ indicating the k-space size of vector. In this study, the magnetic susceptibility artifacts were quantified by controlling TE and material and altering the direction of

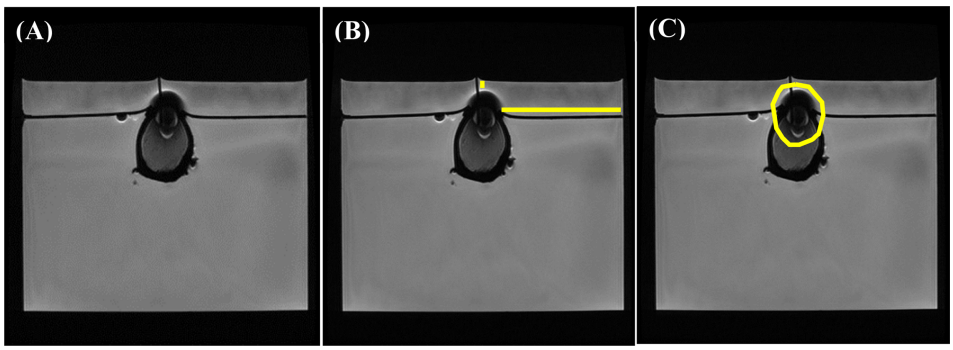

Fig. 3. (Color online) Magnetic susceptibility artifact was measured using an Image J scan in the axial AP direction (A), length measurement in the axial AP image (B), area measurement in the axial AP image (C).

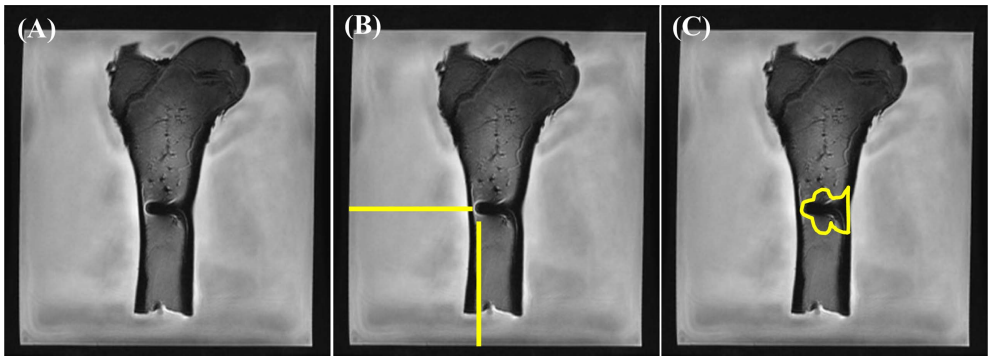

Fig. 4. (Color online) Magnetic susceptibility artifact measurement via Image J scan in the coronal RL direction (A); length measurement in the coronal RL image (B) area measurement in the coronal RL image (C).

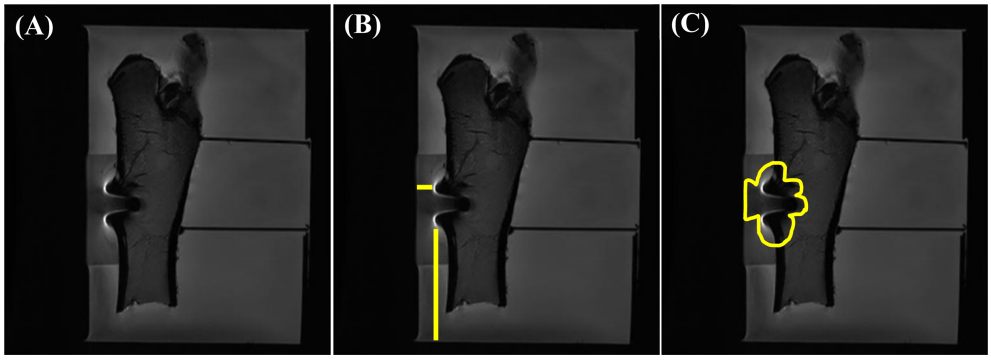

Fig. 5. (Color online) Measurement of magnetic susceptibility artifact via Image J scan in the sagittal AP direction (A); length measurement in the sagittal AP image (B); area measurement in the sagittal AP image (C).

frequency encoding after acquiring images in the axial, coronal, and sagittal planes. The direction of frequency encoding was changed from anterior to posterior (AP) to right to left (RL) in axial, RL was converted to superior to inferior (SI) in the coronal plane, and AP was converted to SI in the sagittal plane. The length and area of the scanned images were measured using Image J (bundled with 32-bit Java 1.6.0_24). The measurements were performed 45 times by five observers, nine times each.

The axial, coronal, and sagittal length measurements were made from areas of magnetic susceptibility artifacts to the brightest part of the distortion. In this case, the artifact length of the axial image was measured from the anterior of the image to the origin of the posterior artifact and the artifact from left to right of the image was measured (Fig. 3).

Artifact length of a coronal image was measured from the inferior of the image to the superior artifact origin and from the right side of the image to the left artifact origin (Fig. 4).

Artifact length of the sagittal image was measured from the inferior to the superior artifact origin and the point anterior to the posterior artifact (Fig. 5).

The magnetic susceptibility artifact area was measured by setting the ROI based on the area of signal loss in the image.

The results of each test were compared with the mean values of the two groups according to the altered frequency-encoding direction using the independent t-test. The SPSS 18.0 (IBM, USA, Chicago) was used for the statistical program. The p value was considered statistically significant when it was less than 0.05.

3. Results

The experimental results of this study involving the axial image suggest that the measured value of anterior-posterior direction was the longest at 5.22 ± 0.159 in the RL frequency-encoding direction and left-right was the longest at 63.68 ± 0.177 in the AP frequency-encoding direction ($p < 0.05$) (Fig. 6). The measured value of magnetic susceptibility artifact area was the maximum at 455.49 ± 2.979 in the RL frequency-encoding direction ($p < 0.05$) (Table 1).

In the coronal plane, the measured value of inferior-superior image was the longest at 58.53 ± 0.125 in the RL

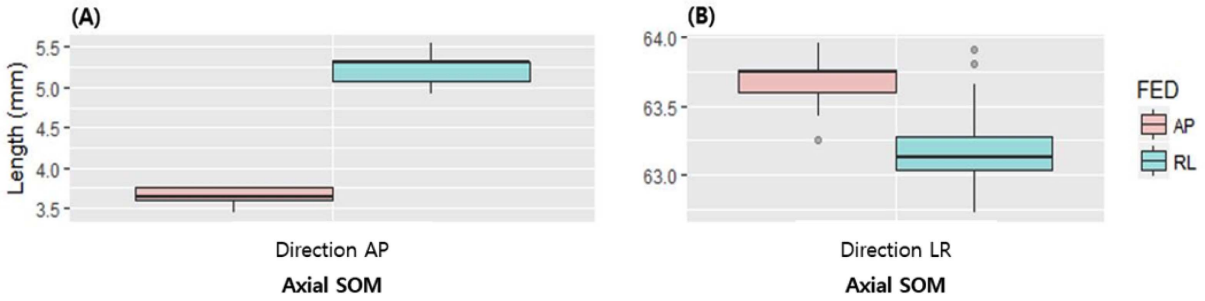

Fig. 6. (Color online) In the axial direction, when the standard length of magnetic susceptibility artifact was set from anterior to posterior, it was the longest when the frequency-encoding direction was RL (A), and when set from left to right, the it was the longest when frequency-encoding direction was AP (B). In this study, SOM stands for standard of measurement and FED refers to Frequency-Encoding Direction.

Table 1. The length and area of the magnetic susceptibility artifact and area in axial images.

Frequency direction	N	Anterior & Posterior (mm)	P	Left & Right (mm)	P	Area (mm^2)	P
AP	45	3.64±0.929	0.000	63.68±0.177	0.000	428.91±2.267	0.000
RL	45	5.22±0.159	0.000	63.16±0.261	0.000	455.49±2.979	0.000

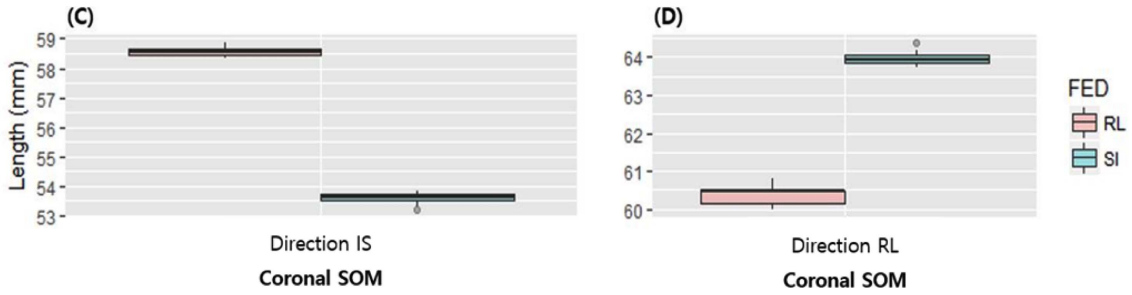

Fig. 7. (Color online) In the coronal direction, when the standard length of magnetic susceptibility artifact was set from inferior to superior, it was the longest when the frequency-encoding direction was RL (C), and when set from right to left, it was the longest when the frequency-encoding direction was SI (D).

frequency-encoding direction, and right-left was to be the longest at 63.97 ± 0.121 in the SI frequency-encoding direction ($p < 0.05$) (Fig. 7). The value of magnetic susceptibility artifact area was the largest at 182.02 ± 1.827 in the RL frequency-encoding direction ($p < 0.05$) (Table 2).

In the sagittal plane, the value of inferior-superior image was the longest at 51.74 ± 0.262 in the AP frequency-encoding direction, and anterior-posterior image was the longest at 8.70 ± 0.172 in the SI frequency-encoding direction ($p < 0.05$) (Fig. 8). The value of magnetic susceptibility artifact area was the largest at 705.17 ± 2.886 in the SI frequency-encoding direction ($p < 0.05$) (Table 3). Fig 9 presents the graphical comparison of magnetic susceptibility artifact area via frequency encoding.

4. Discussion

In patients with fractures, surgical procedures such as screws are used for fixation of metallic implants in the body to minimize the ligament and vascular injury of the

Table 2. The length and area of the magnetic susceptibility artifact and area in coronal Images.

Frequency direction	N	Inferior & Superior (mm)	P	Right & left (mm)	P	Area (mm^2)	P
RL	45	58.53±0.125	0.000	60.35±0.203	0.000	182.02±1.827	0.000
SI	45	53.62±0.127	0.000	63.97±0.121	0.000	155.21±2.554	0.000

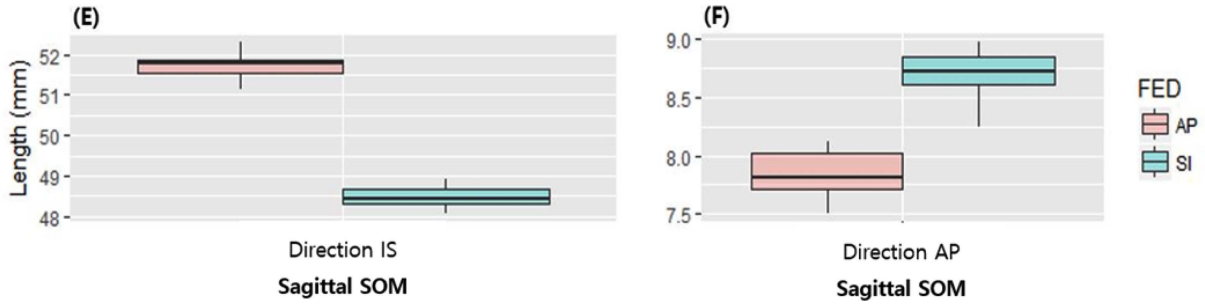

Fig. 8. (Color online) In the sagittal direction, when the standard measurement of length of magnetic susceptibility artifact was set from inferior to superior, it was the longest when the frequency-encoding direction was AP(E), and when set from anterior to posterior, it was the longest when the frequency-encoding direction was SI (F).

Table 3. The length and area of the magnetic susceptibility artifact and area in sagittal images.

Frequency direction	N	Inferior & Superior (mm)	P	Anterior & Posterior (mm)	P	Area (mm^2)	P
AP	45	51.74±0.262	0.000	7.86±0.203	0.000	584.55±2.132	0.000
SI	45	48.49±0.186	0.000	8.70±0.172	0.000	705.17±2.886	0.000

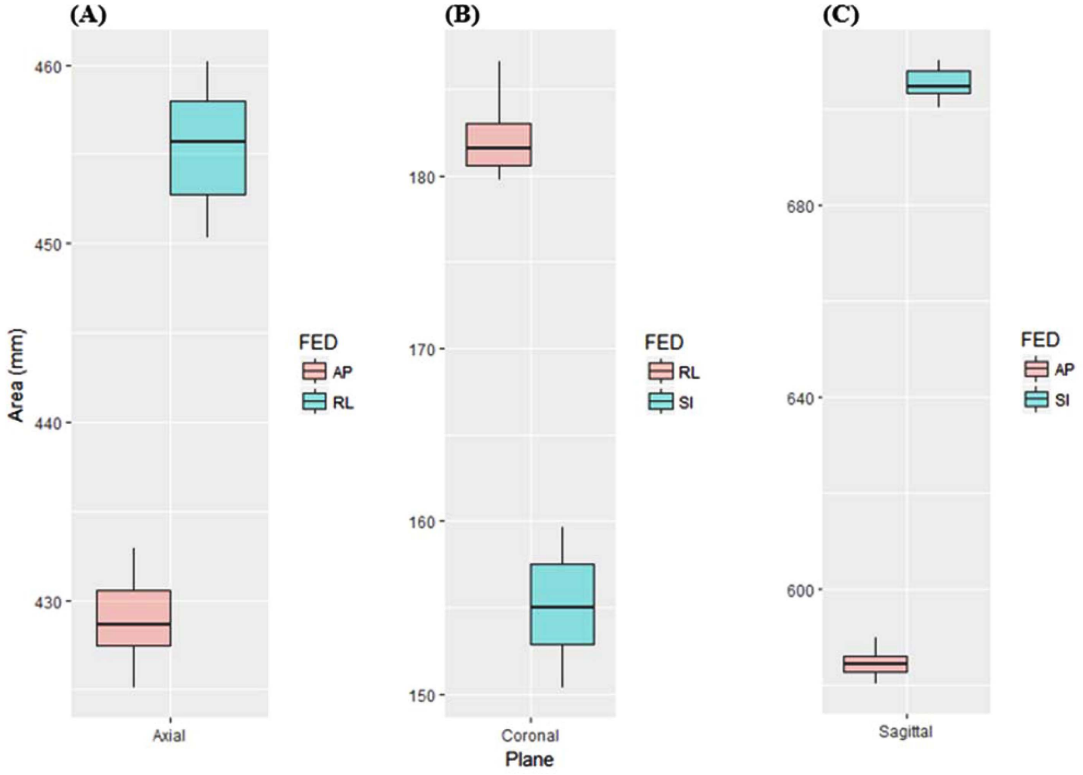

Fig. 9. (Color online) When converting from axial to frequency encoding, magnetic susceptibility artifact was the largest in RL (A). When converting from coronal to frequency encoding, magnetic susceptibility artifact was the largest in RL (B). During the conversion from sagittal plane to frequency encoding, the magnetic susceptibility artifact was the largest in SI (C). In this study, FED refers to Frequency-Encoding Direction.

fractured bone [24].

In patients undergoing screw fixation, the risk of osteoporotic fracture is confirmed via MRI with metal inserts into the body after surgery [25]. Magnetic susceptibility artifacts due to the metal in the human body, results in signal loss, which decreases the diagnostic value of the

image during MRI [26]. The direction of artifact varies depending on the direction of frequency and phase encoding because artifacts follow the direction of matrix alignment [27]. However, many studies investigating image distortion in magnetic susceptibility artifacts failed to quantify the results [28]. Therefore, this study provided basic data pertaining to directionality of magnetic susceptibility artifact by quantifying the length and area of artifact according to the direction of magnetic susceptibility artifact. In the study, magnetic susceptibility artifact length occurred in three directions: axial, coronal, and sagittal based on the direction of frequency encoding.

Cho *et al.* [29] reported the direction of artifact when converting frequency-encoding direction into actual patient values.

In addition [30], the direction of artifact occurred during conversion of the frequency-encoding direction. Cho *et al.* compared the extent of changes in magnetic susceptibility artifacts within the distortion. However, in this study, we measured the length from the end of the image to the point of magnetic susceptibility artifact distortion.

As a result, despite numerical differences the results are consistent with Cho *et al.* In addition, the study investigating changes in magnetic susceptibility artifact area according to the frequency-encoding direction transformation, showed that axial distortion was less in AP than in RL, sagittal distortion was less in AP than SI, and coronal distortion less in SI than RL. Therefore, the length and area of the overall magnetic susceptibility artifact should be carefully determined.

The direction and area of magnetic susceptibility artifacts varied following single screw insertion. Because of the lack of experimental data with various magnetic materials, further studies investigating various types of screws and plates are needed.

5. Conclusion

In this study, it was confirmed that any section showed directionality under altered length and area of magnetic susceptibility artifact. Therefore, determination of the length and area of magnetic susceptibility artifact depending on the direction may be a parameter for investigation during MRI in an environment inducing magnetic susceptibility artifacts.

However, considering the wide range of screws and plates used in screw fixation, additional studies investigating the associated magnetic susceptibility artifact areas are needed. This study represents a basis for the prevention of magnetic susceptibility artifact created by screw fixation.

Acknowledgements

Ji-Won Kim, Wan-Sik Park, Hyun-Sung Kim and Soo-Chul Kim equally contributed to this work; they are co-first authors.

References

[1] K. Abumi, H. Itoh, H. Taneichi, and K. Kaneda, J. Spinal Disord **7**, 1 (1994).
[2] Kevin T. Foley and Sanjay K. Gupta, J. Neurosurg-Spine **1**, 97 (2002).
[3] Y. Kotani, K. Abumi, M. lto, and A. Minami, Eur. Spine J. **14**, 1 (2005).
[4] J. Wang, Y. Zhou, Z. F. Zhang, C. Q. Li, and W. J. Zheng, Eur. Spine J. **22**, 3 (2013).
[5] M. S. Albert, G. D. Catest, and B. Driehuys, Nature **370**, (1994).
[6] G. A. Macdonald and A. J. Peduto, J. Gastroen Hepatol **15**, 9 (2000).
[7] J. Olsrud, J. Latt, and S. B. Kstedt, J. Magn. **22**, 3 (2005).
[8] J. H. Kim, J. Korean Med. Assoc. **53**, 12 (2010).
[9] D. Beyersdorff, K. Taymoorian, T. Knosel, D. Schnorr, R. Felix, B. Hamm, and H. Bruhn, AM J. Roentgenol. **185**, 5 (2005).
[10] S. K. Lee, J. Korean Med. Assoc. **53**, 12 (2010).
[11] D. A. Jimenez, L. J. Armbrust, and R. T. O. Brien, Vet Radiol Ultrasoun **49**, 4 (2008).
[12] F. Shafiei, E. honda, and H. Takahashi, J. Dent. Res. **82**, 8 (2003).
[13] Y. Hirokawa, H. Isoda, and Y. S. Maetani, AM J. Roentgenol **19**, 1 (2008).
[14] L. F. Czervionke, D. L. Daniels, and F. W. Wehrli, AM J. Neuroradiol **9**, 6 (1988).
[15] L. F. Czervionke, D. L. Daniels, F. W. Wehrli, L. P. Mark, L. E. Hendrix, J. A. Strandt, A. L. Williams, and V. M. Haughton, AJNR **9** (1988).
[16] M. L. Wood and R. M. Henkelman, Magn. Reson. Med. **2**, 6 (1985).
[17] K. Farahani, U. Sinha, and S. Sinha, Lect Notes Comput SC **14**, 6 (1990).
[18] Z. Starcuk Jr, H. Hubalkova, and L. Linetskiy, Dent Mater **24**, 6 (2008).
[19] S. Balac and G. Caloz, Comput. Methods Biome. **3**, 4 (2000).
[20] L. Wenmiao, K. Butts Pauly, G. Garry E, P. John M, and H. Bran A, Magn. Reson. Med. **62**, 1 (2009).
[21] A. A. O. Carneiro, G. R. Vilela, D. B. de Araujo, and O. Baffa, Braz. J. Phys. **36**, 1 (2006).
[22] V. Ross D, M. Nathaniel I, R. Meena, U. Sharon E, G. Garry E, G. Nicholas J, M. Albert, S. Greig C, and C. Steven M, Magn. Reson. Med. **56**, 1 (2006).

[23] S. Karin, Z. Jacco A, G. Peter van, L. Tie-Qiang, D. Stephen J, and D. Jeff H, Magn. Reson. Med. **62**, 6 (2009).
[24] A. Ronald I, L. Russell R, V. Robert, and C. Adrian, Neurosurg Focus **8**, 6 (2000).
[25] A. S. Moisala, T. Jarvela, A. Paakkala, T. Paakkala, P. Kannus, and M. Jarvinen, Knee Surg Sport TR A **16**, 12 (2008).
[26] B. Hargreaves, P. W. Worters, K. B. Pauly, J. M. Pauly, K. M. Koch, and G. E. Gold, AM J. Roentgenol. **197**, 3 (2011).
[27] T. Mitsa, K. J. Parker, W. E. Smith, A. M. Tekalp, and J. Szumowski, IEEE T. Med. Imaging **9**, 3 (1990).
[28] F. E. Boada, D. C. Noll, and V. A. Stenger, Magn. Reson. Med. **44** (2000).
[29] C. Jae-Hwan, L. Hae-Kag, and P. Cheol-So, Journal of Digital Contents Society **12**, 1 (2011).
[30] C. Jae Hwan, D. Kyung Rae, C. Woon Kwan, and C. Eun Jin, Journal of Advanced Engineering and Technology **10**, 4 (2017).